Journal of Alloys and Compounds 507 (2010) 535–541

Contents lists available at ScienceDirect

Journal of Alloys and Compounds

journal homepage: www.elsevier.com/locate/jallcom

Microstructure, dielectric and ferroelectric properties of $(1-x)(0.94Bi_{0.5}Na_{0.5}TiO_3-0.06BaTiO_3)-xBiFeO_3$ lead-free ceramics synthesized via a high energy ball milling method

XiaoMing Chen*, XuXu Gong, TingNan Li, Yuan He, Peng Liu

College of Physics and Information Technology, Shaanxi Normal University, Xi'an 710062, People's Republic of China

ARTICLE INFO

Article history:
Received 28 May 2010
Received in revised form 1 August 2010
Accepted 4 August 2010
Available online 12 August 2010

Keywords:
Ceramics
Mechanochemical processing
Electronic properties
Microstructure
SEM
XRD

ABSTRACT

$(1-x)[0.94Bi_{0.5}Na_{0.5}TiO_3-0.06BaTiO_3]-xBiFeO_3$ lead-free ceramics (BNBT–xBFO, $x = 0$, 0.01, 0.03 and 0.07) with fine grain sizes were prepared by solid state reaction of high energy ball milled (HEBM) powders. X-ray diffraction (XRD) patterns exhibited single perovskite structure for the BNBT–xBFO ceramics sintered at an optimum temperature of 1170 °C. Quantitative analysis of the XRD patterns showed that relative amount of tetragonal phase decreased with increasing content of BFO. Due to the effects of HEBM, average grain size of the BNBT–xBFO ceramics was smaller than 1.46 μm and varied with content of BFO. Two dielectric anomalies were observed in $\varepsilon_r - T$ curves. The degree of diffuseness of the phase transition around T_m became more evident with increasing content of BFO. The variation in polarization with BFO amount is consistent with that in mean grain size with BFO amount.

1. Introduction

Lead-free ceramics have attracted considerable attention in recent years owing to the environmental protection concerns. Among various lead-free materials, bismuth sodium titanate ($Bi_{0.5}Na_{0.5}TiO_3$, abbreviated as BNT) is a perovskite ferroelectric with a relatively large remnant polarization ($P_r = 38\ \mu C/cm^2$) and high Curie temperature ($T_c = 320\ ^\circ C$) [1]. Although BNT has been considered to be a promising material as lead-free piezoelectric ceramics, pure BNT ceramics are difficult to pole due to their high conductivity. These drawbacks can be overcome by forming solid solutions with other components. To improve the properties of BNT, more researches have focused on BNT-based solid solutions such as BNT–$(BaSr)TiO_3$ [2], BNT–$BiFeO_3$ [3,4], BNT–Co [5], BNT–Fe_2O_3 [6], BNT–$Bi_{0.5}K_{0.5}TiO_3$ [7,8], BNT–$Bi_{0.5}K_{0.5}TiO_3$–$BiFeO_3$ [9–11], BNT–$Bi_{0.5}K_{0.5}TiO_3$–Sm_2O_3 [12], BNT–$Bi_{0.5}K_{0.5}TiO_3$–$K_{0.5}Na_{0.5}NbO_3$ [13], BNT–$BaTiO_3$ [14–16], BNT–$BaTiO_3$–Bi_2O_3 [17], BNT–$BaTiO_3$–$K_{0.5}Bi_{0.5}TiO_3$ [18,19], BNT–$BaTiO_3$–$CaCO_3$ [20], BNT–$BaTiO_3$–$(K_{0.5}Na_{0.5})NbO_3$ [21–23], BNT–$BaTiO_3$–Mn [24], BNT–$BaTiO_3$–Nb–Co [25], BNT–$BaTiO_3$–Nd_2O_3 [26]. Among them, $(1-x)$BNT–$x BaTiO_3$-based ceramics have attracted much attention because there exists a rhombohedral – tetragonal morphotropic phase boundary (MPB) near $x = 0.06$ [14–26].

For BNT-based ceramics, the large ferroelectricity is always attributed to $(Bi_{0.5}Na_{0.5})^{2+}$ ions, especially Bi^{3+} ions, on the A-site of ABO_3 perovskite structure [27]. In the periodic table, the atomic weight of Bi is as large as that of Pb and the electronic configuration of Bi^{3+} is identical to that of Pb^{2+}. So, addition of Bi-based ferroelectrics will play a key role in BNT-based ceramics. Among the Bi-based ferroelectrics, bismuth ferrite ($BiFeO_3$, abbreviated as BFO) has ABO_3 perovskite structure and ferroelectricity with high Curie temperature ($T_c = 836\ ^\circ C$) [28].

High energy ball milling (HEBM) has been used to synthesize nanometer powders successfully [29]. By solid state reaction combined with HEBM technique, ceramics with fine grain size can be obtained [30,31]. In this paper, $0.94Na_{0.5}Bi_{0.5}TiO_3$–$0.06BaTiO_3$ (abbreviated as BNBT) was selected as a representative composition, and BFO was chosen as a third component. By means of solid state reaction of HEBM precursor powders, $(1-x)(0.94Na_{0.5}Bi_{0.5}TiO_3-0.06BaTiO_3)-xBiFeO_3$ (abbreviated as BNBT–xBFO) lead-free ceramics with fine grain size were prepared. The effects of BFO on their microstructure, dielectric and ferroelectric properties were investigated.

2. Experimental procedures

$(1-x)(0.94Bi_{0.5}Na_{0.5}TiO_3-0.06BaTiO_3)-xBiFeO_3$ (BNBT–xBFO, $x = 0$, 0.01, 0.03 and 0.07) ceramics were prepared by solid state reaction of HEBM precursor pow-

* Corresponding author. Tel.: +86 29 85303823; fax: +86 29 85303823.
E-mail addresses: xmchen-snnu@163.com, xmchen@snnu.edu.cn (X. Chen).

0925-8388/$ – see front matter © 2010 Elsevier B.V. All rights reserved.
doi:10.1016/j.jallcom.2010.08.012

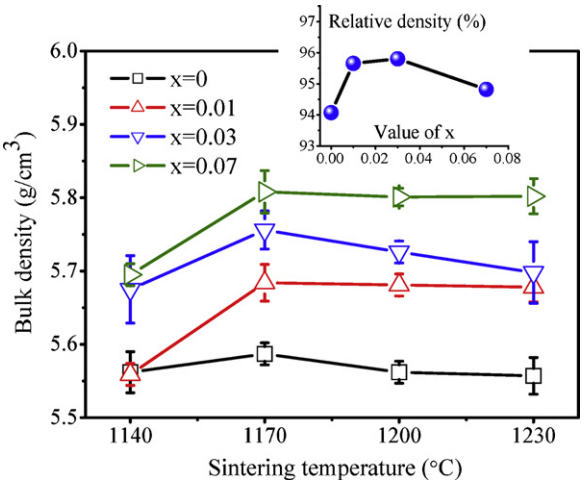

Fig. 1. Bulk density of the BNBT–*x*BFO ceramics as a function of sintering temperature. The inset shows relative density of the BNBT–*x*BFO ceramics sintered at 1170 °C as a function of *x*.

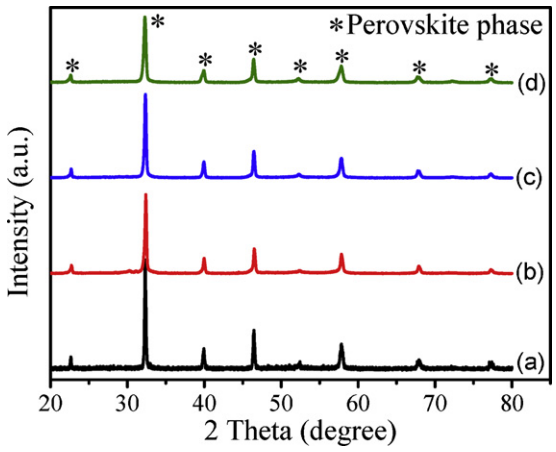

Fig. 2. XRD patterns of the BNBT–*x*BFO ceramics sintered at 1170 °C: (a) $x = 0$, (b) $x = 0.01$, (c) $x = 0.03$ and (d) $x = 0.07$.

ders. Analytical grade $BaCO_3$, TiO_2, Na_2CO_3, Bi_2O_3, and Fe_2O_3 in stoichiometric ratio of the compositions were put in agate vials with agate balls and milled for 5 h in Fritsch Vario-Planetary HEBM system in air. Rotation speed of the disk was 300 rpm and that of the vials was 450 rpm. The milled powders were subsequently calcined at 800 °C for 2 h. The calcined powders were pulverized with approximately 5 wt% polyvinyl alcohol. Pellets of 11.5 mm in diameter and approximately 1.5 mm in thickness were pressed under uniaxial pressure of 200 MPa and burned out the binder at 500 °C for 2 h. The pellets were sintered between 1140 °C and 1230 °C for 2 h, at heating and cooling rates of 3 °C/min. In order to prevent the volatilitization of Bi and Na, all pellets were embedded in the powders with the same composition and placed in covered alumina crucibles during the sintering process.

Bulk density of the ceramics was measured by Archimedes method and relative density was calculated. Crystal structure of the ceramics was investigated by X-ray diffraction (XRD, Rigaku D/Max 2550) at a step size of 0.01° using a Cu K_α radiation. Microstructure of the sintered samples was observed by scanning electron microscope (Quanta 200 SEM, FEI Co., Eindhoven, Netherlands) with energy dispersive spectrometer (EDS). Average size of grains was determined by the line intersect method.

Silver electrodes were coated and fired at 650 °C for 15 min for electrical characterization. Dielectric measurement was performed by using an Agilent E4980A precision LCR from room temperature to 500 °C. Ferroelectric hysteresis loops were measured at 50 Hz in silicon oil with a radiant precision workstation ferroelectric testing system. Maximum polarization (P_m), remnant polarization (P_r) and coercive filed (E_c) were determined from the *P*–*E* hysteresis loops.

3. Results and discussion

Fig. 1 shows the dependences of the bulk densities of the BNBT–*x*BFO ceramics as a function of sintering temperature. For all BNBT–*x*BFO ceramics, the bulk densities increase to their maximum values as the sintering temperature is increased from 1140 °C to 1170 °C, and then drop slightly with further increasing sintering temperature. At a given sintering temperature, the higher the amount of BFO is contained, the higher the bulk density the sample has. It is known that the substitution site is mainly determined by ionic radius and charge. Though the charge of Fe^{3+} ion differs from that of Ti^{4+}, the radius of Fe^{3+} ion (0.65 Å) is compatible with that of Ti^{4+} ion (0.61 Å) [32]. So, Fe^{3+} ions should substitute Ti^{4+} ions. The atomic weight of Fe (55.85 g/mol) is larger than that of Ti (47.90 g/mol). Thus, bulk densities of the BNBT–*x*BFO ceramics sintered at same temperature increase with increasing content of BFO. Bulk densities of the BNBT–*x*BFO ceramics decrease when the sintering temperature is higher than 1170 °C. Therefore, the optimum sintering temperature is 1170 °C. The dependence of the relative densities of the BNBT–*x*BFO ceramics sintered at 1170 °C for 2 h as a function of *x* is shown in the inset of Fig. 1. The relative density gradually increases with increasing *x* and reaches a maximum value of 95.8% at $x = 0.03$. Then, the relative density decreases with increasing *x* to 0.07. Although relative density of the BNBT ceramics ($x = 0$) is smallest, it is still above 94%. This suggests that all BNBT–*x*BFO ceramics were well sintered at 1170 °C. It also indicates that there is an optimum amount of BFO in promoting sintering behavior of the BNBT–*x*BFO ceramics.

Fig. 2 shows XRD patterns of the BNBT–*x*BFO ceramics sintered at 1170 °C for 2 h. It is found that all ceramics exhibit typical diffraction peaks of ABO_3 perovskite phase. No second phase is observed, suggesting that all Bi^{3+} and Fe^{3+} ions have dissolved into the lattice structure of BNBT to form solid solutions.

In the ceramics with the composition near $0.94(Na_{0.5}Bi_{0.5})TiO_3$–$0.06BaTiO_3$ there is a rhombohedral – tetragonal MPB [14]. XRD patterns of the composition at MPB are characterized with the presence of (0 0 3)/(0 2 1) two peaks between 38.5° and 41.0° and the splitting of the peak (2 0 2) between 45.0° and 47.5° [10,26]. In this experiment, the composition of the BNBT–*x*BFO ceramics was selected at MPB. Further XRD analysis for the BNBT–*x*BFO ceramics performed in the 2θ ranges of 38.5–41.0° and 45.0–47.5° is shown in Fig. 3. Although the splitting of the XRD peaks is not very obvious except the peak between 38.5° and 41.0° with $x = 0.07$, all peaks are asymmetrical. To characterize the phase compositions in a more quantitative way, the peaks were fitted by Peakfit software using the least-squares approach. In order to obtain smaller values of residual factor, the peak shape was modeled by a Pearson-VII function taking into account both Lorentzian and Gaussian functions. The peaks between 38.5° and 41.0° were fitted into $(0\,0\,3)_R/(0\,2\,1)_R$ peaks, and the peaks between 45.0° and 47.5° were fitted into $(2\,2\,0)_T$ and $(2\,0\,2)_R$ peaks, where R and T denote rhombohedral and tetragonal phase, respectively. The results indicate that MPB still appears in the BNBT-based ceramics after adding various amounts of BFO. The relative amount of tetragonal phase was determined by the following equation:

$$\text{tetragonal}\,\% = \frac{\text{area}(2\,2\,0)_T}{\text{area}(2\,2\,0)_T + \text{area}(2\,0\,2)_R}$$

The relative amounts of tetragonal phase are 48.2%, 44.4%, 42.7% and 38.2% for the BNBT–*x*BFO ceramics with $x = 0$, 0.01, 0.03 and 0.07, respectively. That is to say, with increasing content of BFO, relative amount of tetragonal phase is decreased.

Fig. 4(a–d) shows SEM images of the surfaces of the BNBT–*x*BFO ceramics sintered at 1170 °C for 2 h. It can be seen that the BNBT–*x*BFO ceramics have a fine and homogeneous microstructure. Almost no pores are found on surface and all ceramics are dense. By means of the intercept method, mean grain sizes of the BNBT–*x*BFO ceramics with $x = 0$, 0.01, 0.03 and 0.07 were deter-

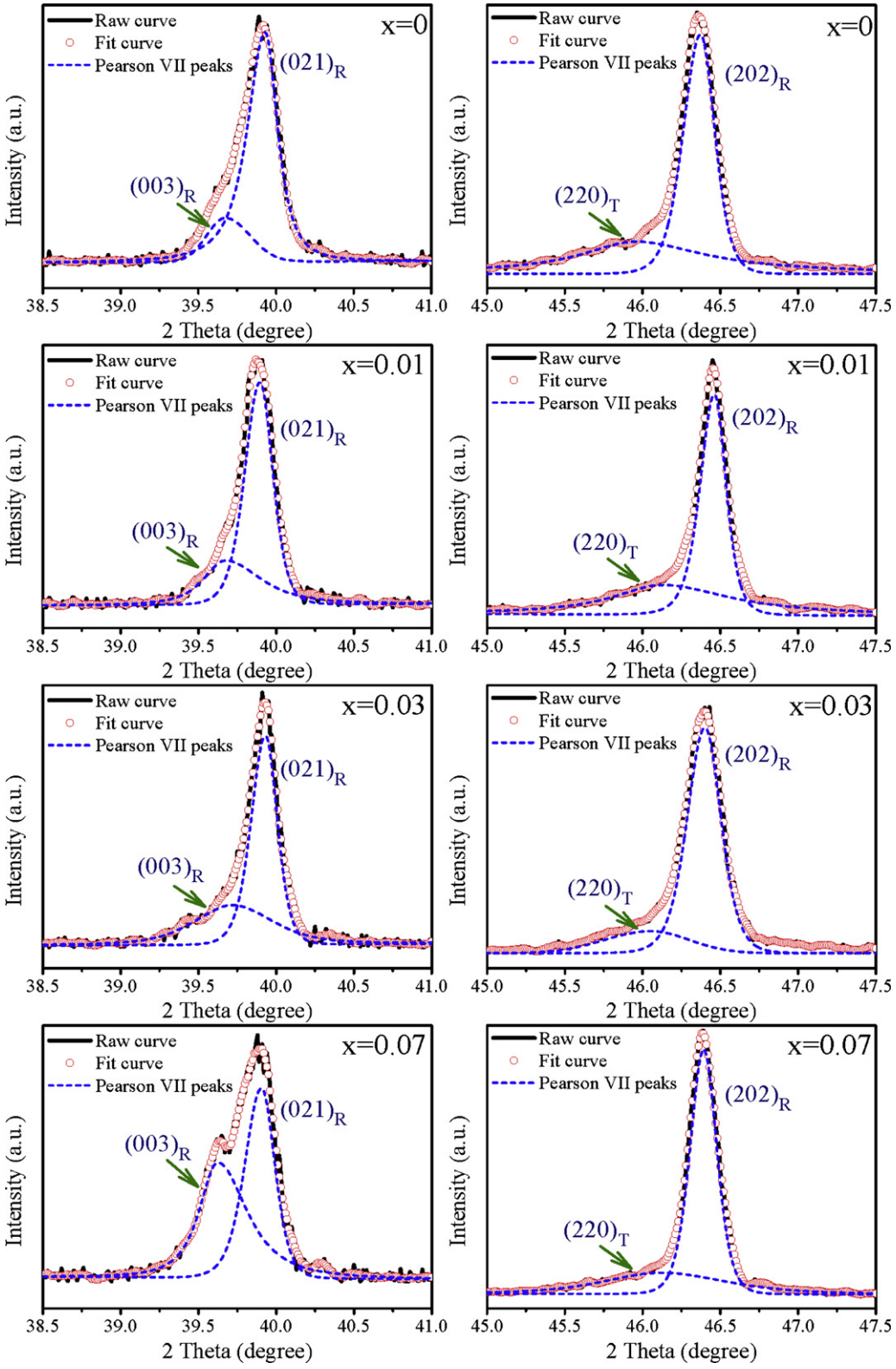

Fig. 3. XRD fitting patterns of the BNBT–*x*BFO ceramics sintered at 1170 °C in the 2θ ranges of 38.5–41.0° and 45.0–47.5°.

mined to be 1.04, 1.20, 1.46 and 1.16 μm, respectively. Compared to those of the BNBT–0BFO ceramics, average grain sizes of the ceramics with $x = 0.01$ and $x = 0.03$ are increased. The increase of grain sizes can be attributed to the presence of BFO which greatly improved the sintering behavior and significantly promoted densification of the ceramics (see the inset of Fig. 1). Similar phenomenon was also observed in BFO modified $Bi_{0.5}Na_{0.5}TiO_3$–$Bi_{0.5}K_{0.5}TiO_3$ ceramics [10] and Nd_2O_3 doped $(Bi_{0.5}Na_{0.5})_{0.94}Ba_{0.06}TiO_3$ ceramics [26]. However, grain growth was inhibited with further doping of BFO ($x = 0.07$). EDS results show that Fe^{3+} concentrates near grain boundaries in the BNBT–7BFO ceramics (not shown here). The reduction in grain size of the BNBT–7BFO ceramics can be attributed

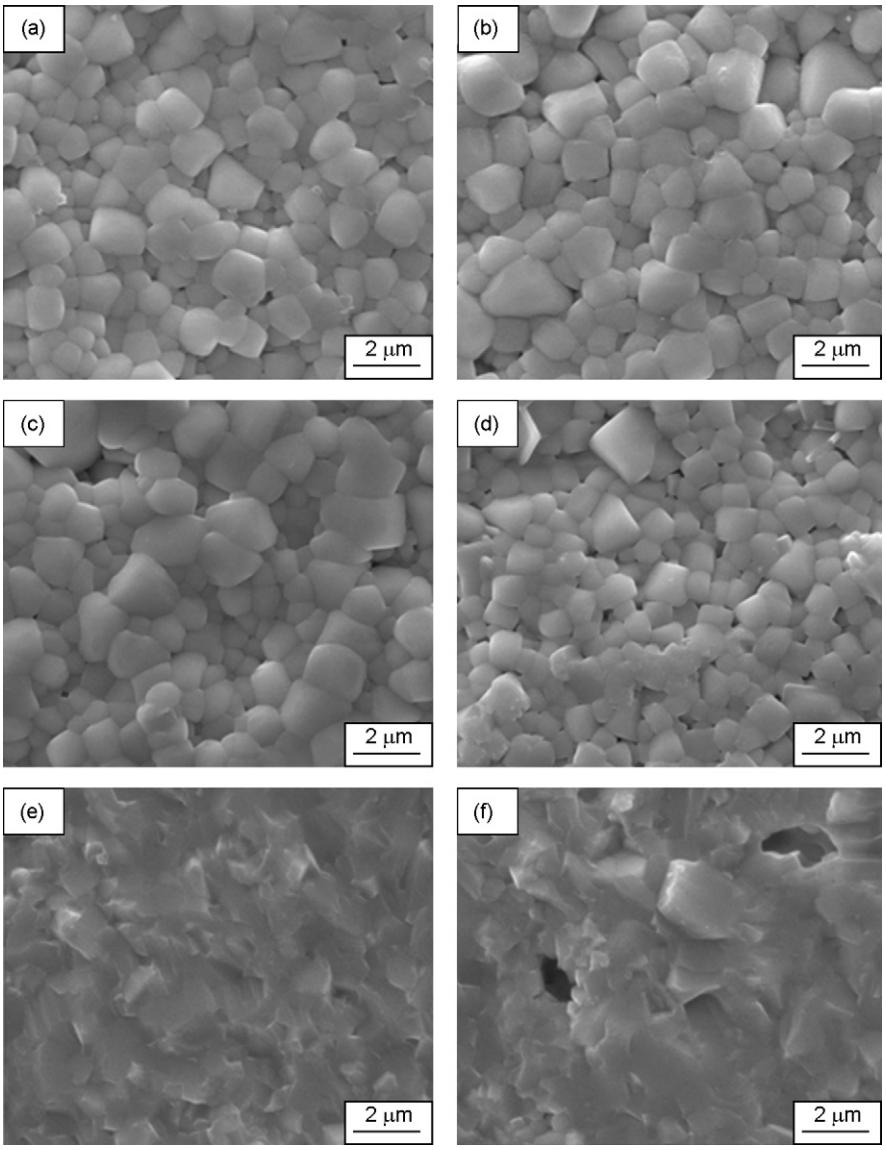

Fig. 4. SEM images of the surfaces of the BNBT–*x*BFO ceramics sintered at 1170 °C: (a) $x = 0$, (b) $x = 0.01$, (c) $x = 0.03$, (d) $x = 0.07$; and fractures of the BNBT–3BFO ceramics sintered at 1170 °C (e) and 1200 °C (f).

to the presence of Fe^{3+} near grain boundaries, which inhibited grain growth.

For all samples, the average grain size is smaller than 1.46 μm. The average grain size of the ceramics obtained here is always smaller than that of the BNBT-based ceramics prepared by the conventional solid state reaction process [26,33]. For example, the average grain size of the BNBT ($x = 0$) ceramics in our experiment is about 1.04 μm, which is smaller than that of the ceramics with the same composition obtained by the conventional solid state reaction process (about 2 μm) [33]. It is believed that low calcination temperature is beneficial to fine grain size of ceramics [29,30]. HEBM improved reaction activity of the milled powders and thus lowered calcination temperature. In our experiment, the calcination temperature of 800 °C for obtaining single phase BNBT–*x*BFO from the HEBM precursor powders is lower than that required by the conventional solid state reaction process [33]. So, the fine grain size of the BNBT–*x*BFO ceramics can be mainly attributed to the effects of HEBM. Fig. 4(e–f) shows typical SEM micrographs of the fractures of the BNBT–3BFO ceramics sintered at 1170 °C and 1200 °C, respectively. It can be seen that almost no pores are observed in the BNBT–3BFO ceramics sintered at 1170 °C. As the sintering temperature was increased to 1200 °C, there appeared a few pores in the body of the ceramics. Therefore, bulk densities of the ceramics decreased when the sintering temperature was higher than 1170 °C (Fig. 1).

Fig. 5 shows variations in dielelctric constant (ε_r) and dielectric loss ($\tan\delta$) of the BNBT–*x*BFO ceramics sintered at 1170 °C for 2 h as a function of temperature (T). The curves of $\varepsilon_r - T$ and $\tan\delta - T$ for all ceramics are similar. Two dielectric anomalies are observed in the $\varepsilon_r - T$ curves. The first dielectric anomaly locates at about 140–170 °C, denoted as T_d, which is caused by the phase transition between ferroelectric state and so-callled ″anti-ferroelectric″ state. The second one corresponding to the maximum value of ε_r is at temperatures of about 290–312 °C (denoted as T_m), which is associated with the phase transition between ″anti-ferroelectric″ state and paraelectric state. The dependences of ε_r on frequency are different in different ranges of temperature. As the temperature is above T_m, the frequency dependence becomes significant and ε_r drops obviously with increasing frequency. The $\tan\delta - T$ curves exhibit one peak at temperatures of about 100–140 °C, denoted as T_f, which locates at a temperature below T_d. Around T_f, the $\tan\delta$ measured at lower frequencies is lower than that

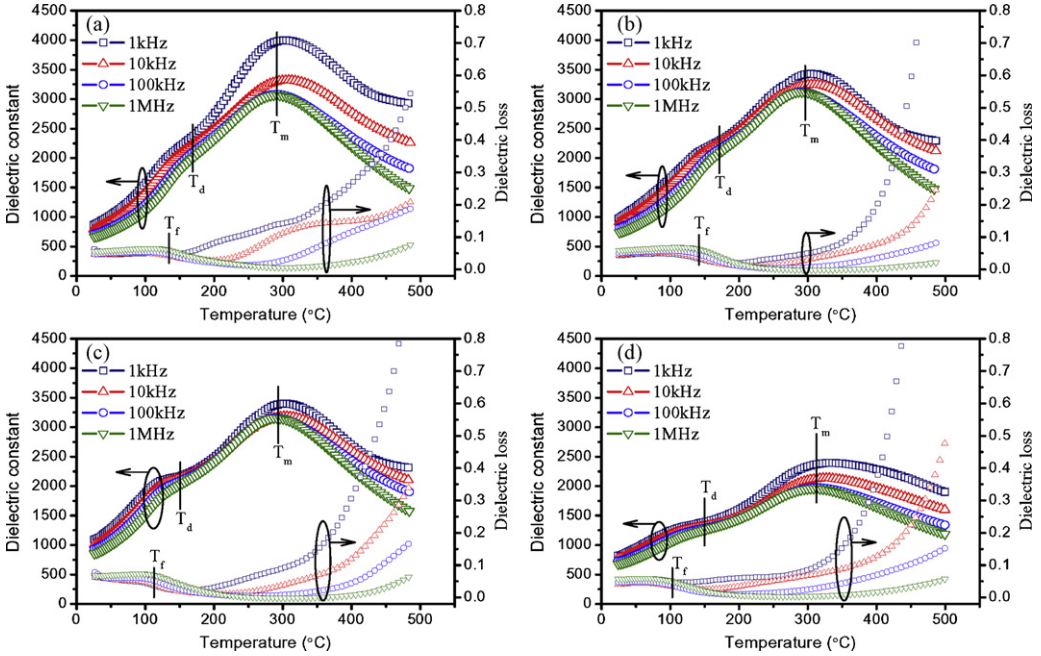

Fig. 5. Dielectric constant and dielectric loss of the BNBT–*x*BFO ceramics sintered at 1170 °C vs. temperature at frequencies of 1, 10, 100 and 1000 kHz: (a) $x = 0$, (b) $x = 0.01$, (c) $x = 0.03$ and (d) $x = 0.07$.

measured at higher frequencies for all ceramics. With further increasing temperature (around T_m), the tanδ measured at lower frequencies is larger than that measured at higher frequencies. Similar phenomena were also observed in other BNT-based ceramics [11,26].

The dependence of dielectric properties on frequency is associated with many factors such as interfacial polarization, microscopic composition fluctuation, order–disorder transition, macrodomain and microdomain switching, and so on [34]. The T_m does not exhibit obvious upshift with increasing frequencies, which is different from classic relaxor characteristics [11]. It should be noted that the maximum value of ε_r is reduced when the amount of BFO is superabundant ($x = 0.07$), suggesting that dielectric properties were weakened. The value of T_m increases from 290 °C to 312 °C with increasing x from 0 to 0.07. This is mainly due to the high Curie temperature for BFO (836 °C).

The $\varepsilon_r - T$ curves of the BNBT–*x*BFO ceramics exhibit broad dielectric peaks around T_m, which implies the characteristic of diffuse phase transition. In order to further characterize the dielectric dispersion and diffuseness of the phase transition, a modified Curie–Weiss law proposed by Uchino and Nomura [35] was employed: $1/\varepsilon_r - 1/\varepsilon_m = (T - T_m)^\gamma/C'$, where ε_m is the maximum value of dielectric constant at the phase transition temperature T_m, C' is the Curie-like constant, and γ is the degree of diffuseness. γ is usually ranging from 1 for a normal ferroelectric to 2 for an ideal relaxor ferroelectric. Plots of $\mathrm{Ln}(1/\varepsilon_r - 1/\varepsilon_m)$ as a function of $\mathrm{Ln}(T - T_m)$ at 100 kHz of the BNBT–*x*BFO ceramics are shown in Fig. 6. All samples exhibit a linear characteristic. By least-squared

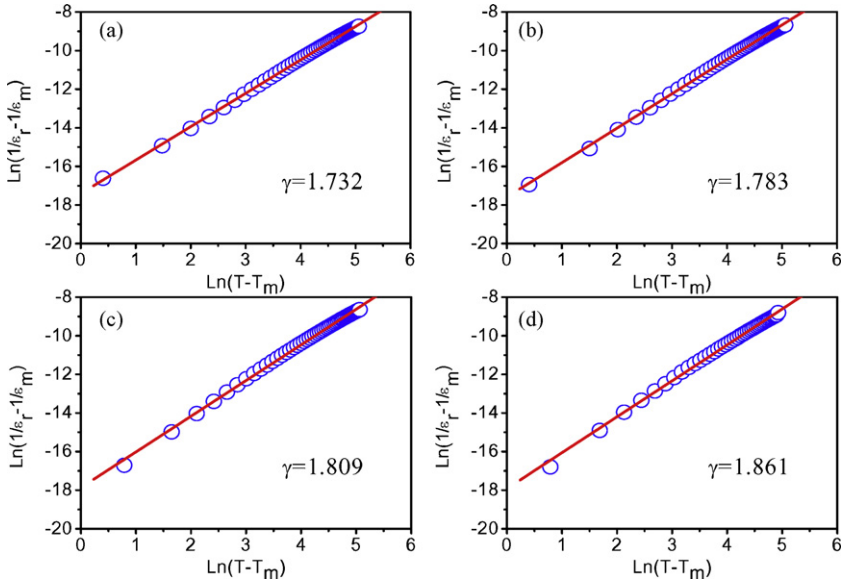

Fig. 6. Plots of $\mathrm{Ln}(1/\varepsilon_r - 1/\varepsilon_m)$ vs. $\mathrm{Ln}(T - T_m)$ of the BNBT–*x*BFO ceramics sintered at 1170 °C: (a) $x = 0$, (b) $x = 0.01$, (c) $x = 0.03$ and (d) $x = 0.07$. The symbols denote experimental data measured at 100 kHz, while the solid lines denote the least-squared fitting curves to the modified Curie–Weiss law.

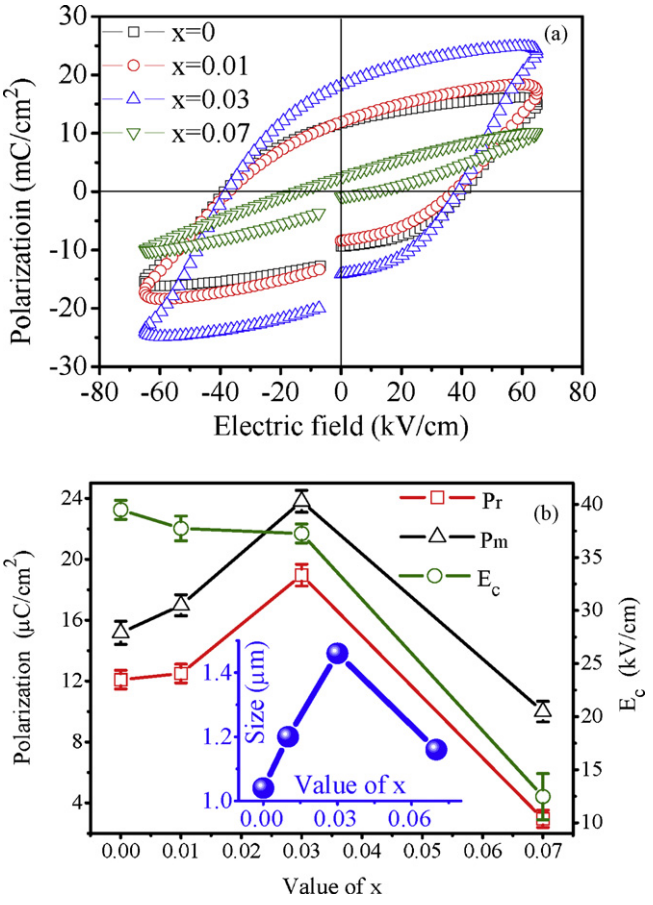

Fig. 7. *P–E* loops of the BNBT–*x*BFO ceramics sintered at 1170 °C measured at 50 Hz (a), and variation of P_m, P_r and E_c as a function of *x* (b). The inset in (b) shows mean grain size of the BNBT–*x*BFO ceramics as a function of *x*.

fitting the experimental data to the modified Curie–Weiss law, γ was determined. The value of γ is increased from 1.732 to 1.861 with *x* from 0 to 0.07. This suggests that the degree of the diffuseness of the phase transition is enhanced with increasing amount of BFO. This phenomenon can be attributed to distortion of the unit cell [11]. With the substitutions of Fe^{3+} ions for Ti^{4+} ions and Bi^{3+} ions entering into A-site of the perovskite structure, the unit cell was distorted and thus the dipolar moment was changed. Crystal structure and chemical composition became more inhomogeneous with increasing substitution concentration, so that degree of diffuseness of the phase transition became more evident.

Fig. 7(a) shows polarization vs. electric field of the BNBT–*x*BFO ceramics measured at 50 Hz. Clear hysteresis loops are observed for all samples, which are typical shapes of ferroelectric materials. Fig. 7(b) depicts variations of P_m, P_r and E_c as a function of *x*. With increasing amount of BFO, both P_m and P_r increase and then decrease. E_c decreases with increasing amount of BFO. The BNBT–0.03BFO ceramics exhibit highest P_r and P_m of 18.96 μC/cm^2 and 23.81 μC/cm^2, respectively, and intermediate E_c of 37.26 kV/cm at 70 kV/cm. With further increasing *x* to 0.07, *P–E* loop becomes narrow, indicating that ferroelectric properties of the BNBT–0.07BFO ceramics are decreased as compared to the samples with $x < 0.07$. It can be seen that the variation in polarization with *x* is the same as that in mean grain size with *x* (see the inset of Fig. 7(b)). Buessem et al. [36] reported that the coupling between grain boundaries and domain walls in fine-grained ceramics was stronger than that in coarse-grained ones. The strong coupling induced a decrease in domain wall mobility and in achievable domain alignment. So, polarization of the ceramics with reduced grain size is decreased. As observed from the hysteresis curves, the doping of BFO significantly influences the loops shape and polarization values. This suggests that the ferroelectric order of BNBT was disrupted by the addition of BFO. With diffusing of BFO into BNBT lattice structure and possible volatilitization of Bi^{3+} during high temperature sintering, A-site vacancies would be created. These A-site vacancies facilitated the movement of the ferroelectric domain and made the polarization switching easier [4]. However, Fe^{3+} substituted B-sites, which would result in an increase in oxygen vacancy concentration. Oxygen vacancies are unfavorable to polarization switching, leading to a decrease in Pr [37]. On the other hand, with increasing amount of BFO, the relative amount of tetragonal phase in the BNBT–*x*BFO ceramics is decreased (Fig. 3). Liu et al. have found that an increase in tetragonal phase in the BNBT-based ceramics was propitious to improvement of electrical properties [38]. We attribute the dependence of ferroelectric properties on the amount of BFO to the competitive effects of many factors, such as A-site vacancy, oxygen vacancy, percentage of tetragonal phase and grain size. The exact mechanism will be further studied in our future work.

4. Conclusions

Microstructure, dielectric and ferroelectric properties of the BNBT–*x*BFO ceramics with fine grain size, synthesized by solid state reaction of HEBM powders, were studied. The dense ceramics sintered at 1170 °C had a mean grain size of less than 1.46 μm. XRD analysis showed that the relative amount of tetragonal phase decreased with increasing amount of BFO. Microstructure, dielectric and ferroelectric properties of the BNBT–*x*BFO ceramics were affected by the amount of BFO. The degree of diffuseness of the phase transition around T_m became more evident with increasing content of BFO. It is suggested that the variation in polarization with BFO amount is associated with many factors such as A-site vacancy, oxygen vacancy, percentage of tetragonal phase and grain size.

Acknowledgements

This work was supported by the Fundamental Research Funds for the Central Universities (No. GK200902054), Laboratory Opening-Found for College Students in Shaanxi Normal University (No. 2010056) and Shaanxi Normal University Work-Study Programme for Scientific Research Innovation Fund (QZZD10078).

References

[1] G.A. Smolenskii, V.A. Isupov, A.I. Agranovskaya, N.N. Krainik, Sov. Phys. Solid State 2 (1961) 2651–2654.
[2] W.C. Lee, C.Y. Huang, L.K. Tsao, Y.C. Wu, J. Alloys Compd. 492 (2010) 307–312.
[3] V. Dorcet, P. Marchet, G. Trolliard, J. Eur. Ceram. Soc. 27 (2007) 4371–4374.
[4] E.V. Ramana, S.V. Suryanarayana, T.B. Sankaram, Solid State Sci. 12 (2010) 956–962.
[5] Y.G. Wang, G. Xu, X.P. Ji, Z.H. Ren, W.J. Weng, P.Y. Du, G. Shen, G.R. Han, J. Alloys Compd. 475 (2009) L25–L30.
[6] E. Aksel, E. Erdem, P. Jakes, J.L. Jones, R.A. Eichel, Appl. Phys. Lett. 97 (2010), 012903~1–012903~3.
[7] X.M. Chen, Y.W. Liao, H.P. Wang, L.J. Mao, D.Q. Xiao, J.G. Zhu, Q. Chen, J. Alloys Compd. 493 (2010) 368–371.
[8] Y.M. Li, R.H. Liao, X.P. Jiang, Y.P. Zhang, J. Alloys Compd. 484 (2009) 961–965.
[9] M.J. Zou, H.Q. Fan, L. Chen, W.W. Yang, J. Alloys Compd. 495 (2010) 280–283.
[10] C.R. Zhou, X.Y. Liu, W.Z. Li, C.L. Yuan, Mater. Chem. Phys. 114 (2009) 832–836.
[11] C.R. Zhou, X.Y. Liu, W.Z. Li, C.L. Yuan, Solid State Commun. 149 (2009) 481–485.
[12] Y.J. Zhang, R.Q. Chu, Z.J. Xu, J.G. Hao, Q. Chen, F. Peng, W. Li, G.R. Li, Q.R. Yin, J. Alloys Compd. 502 (2010) 341–345.
[13] K.T.P. Seifert, W. Jo, J. Rodel, J. Am. Ceram. Soc. 93 (2010) 1392–1396.
[14] Y.S. Sung, J.M. Kim, J.H. Cho, T.K. Song, M.H. Kim, T.G. Park, Appl. Phys. Lett. 96 (2010), 202901~1–202901~3.
[15] M. Cernea, E. Andronescu, R. Radu, F. Fochi, C. Galassi, J. Alloys Compd. 490 (2010) 690–694.
[16] D.Z. Zhang, X.J. Zheng, X. Feng, T. Zhang, J. Sun, S.H. Dai, L.J. Gong, Y.Q. Gong, L. He, Z. Zhu, J. Huang, X. Xu, J. Alloys Compd. 504 (2010) 129–133.
[17] M.L. Liu, Y.F. Qu, D.A. Yang, J. Alloys Compd. 503 (2010) 237–241.

[18] C.W. Tai, Y. Lereah, Appl. Phys. Lett. 95 (2009) 062901–062903.
[19] Y.J. Dai, S.J. Zhang, T.R. Shrout, X.W. Zhang, J. Am. Ceram. Soc. 93 (2010) 1108–1113.
[20] S.N. Yun, X.L. Wang, J. Shi, D.L. Xu, J. Alloys Compd. 485 (2009) 610–615.
[21] X. Tan, E. Aulbach, W. Jo, T. Granzow, J. Kling, M. Marsilius, H.J. Kleebe, J. Rödel, J. Appl. Phys. 106 (2009), 044107∼1–044107∼7.
[22] J.E. Daniels, W. Jo, J. Rödel, V. Honkimäki, J.L. Jones, Acta Mater. 58 (2010) 2103–2111.
[23] S.T. Zhang, A.B. Kounga, W. Jo, C. Jamin, K. Seifert, T. Granzow, J. Rödel, D. Damjanovic, Adv. Mater. 21 (2009) 1–5.
[24] Q.H. Zhang, Y.Y. Zhang, F.F. Wang, Y.J. Wang, D. Lin, X.Y. Zhao, H.S. Luo, W.W. Ge, D. Viehland, Appl. Phys. Lett. 95 (2009), 102904∼1–102904∼3.
[25] H.I. Hsiang, L.T. Mei, Y.J. Chun, J. Am. Ceram. Soc. 92 (2009) 2768–2771.
[26] P. Fu, Z.J. Xu, R.Q. Chu, W. Li, G.Z. Zang, J.G. Hao, Mater. Sci. Eng. B 167 (2010) 161–166.
[27] Z. Yu, V.D. Krstic, B.K. Mukherjee, J. Mater. Sci. 42 (2007) 3544–3551.
[28] G.A. Smolenskii, I. Chupis, Sov. Phys. Usp. 25 (1982) 475–493.
[29] L.B. Kong, T.S. Zhang, J. Ma, F. Boey, Prog. Mater. Sci. 53 (2008) 207–322.
[30] X.M. Chen, P. Liu, J.P. Zhou, W.W. Kong, J.W. Zhang, Physica B 405 (2010) 2815–2819.
[31] Z.F. Fu, P. Liu, X.M. Chen, J.L. Ma, H.W. Zhang, J. Alloys Compd. 493 (2010) 441–444.
[32] R.D. Shannon, Acta Crystallogr. A 32 (1976) 751–767.
[33] C.G. Xu, D.M. Lin, K.W. Kwok, Solid State Sci. 10 (2008) 934–940.
[34] X.Y. Wei, Y.J. Feng, X. Yao, Appl. Phys. Lett. 83 (2003) 2031–2033.
[35] K. Uchino, S. Nomura, Ferroelectrics 44 (1982) 55–61.
[36] W.R. Buessem, L.E. Cross, A.K. Goswami, J. Am. Ceram. Soc. 49 (1966) 33–36.
[37] T. Friessnegg, S. Aggarwal, R. Ramesh, B. Nielsen, E.H. Poindexter, D.J. Keeble, Appl. Phys. Lett. 77 (2000) 127–129.
[38] L.J. Liu, H.Q. Fan, S.M. Ke, X.L. Chen, J. Alloys Compd. 458 (2008) 504–508.